

Soft Matter

Accepted Manuscript



This is an *Accepted Manuscript*, which has been through the Royal Society of Chemistry peer review process and has been accepted for publication.

Accepted Manuscripts are published online shortly after acceptance, before technical editing, formatting and proof reading. Using this free service, authors can make their results available to the community, in citable form, before we publish the edited article. We will replace this *Accepted Manuscript* with the edited and formatted *Advance Article* as soon as it is available.

You can find more information about *Accepted Manuscripts* in the [Information for Authors](#).

Please note that technical editing may introduce minor changes to the text and/or graphics, which may alter content. The journal's standard [Terms & Conditions](#) and the [Ethical guidelines](#) still apply. In no event shall the Royal Society of Chemistry be held responsible for any errors or omissions in this *Accepted Manuscript* or any consequences arising from the use of any information it contains.



Journal Name

ARTICLE

Two Bent-Shaped π -Organogelators: Synthesis, Fluorescence, Self-Assembly and Detection of Volatile Acid Vapours in Gel Films and in Gel-Gel States

Received 00th January 20xx,
Accepted 00th January 20xx

DOI: 10.1039/x0xx00000x

www.rsc.org/

Xiaomin Qian, Weitao Gong*, Manivannan Kalavathi Dhinakaran, Peng Gao, Duo Na, and Guiling Ning*

Two novel bent-shaped π -organogelators **6a** and **6b** having different terminal pyridine ring as responsive site were designed, synthesized and fully characterized. A subtle difference in the position of the N atom at pyridine ring greatly affected their fluorescence and gelation properties. **6b** showed remarkably stronger fluorescence both in solution and in solid state as compared to **6a**. Theoretical calculation revealed a clear discrepancy of electron distribution between them. Furthermore, driven by π - π stacking interaction and hydrophobic interaction, both **6a** and **6b** can gelate several organic solvents with different polarities. Rheological studies, spectroscopic tests and powder X-ray diffraction showed that **6a** displayed a closer stacking mode leading to stronger gel robustness. The xerogel films of **6a** and **6b** were prepared and utilized to detect acid vapours. Both of them can fulfil the detection of acid vapours through a distinct fluorescence change which could be seen by naked eye under UV lamp, but with different sensing modes. A rare gel to gel transformation was also observed upon exposure to acid vapours accompanied with a morphological change.

Introduction

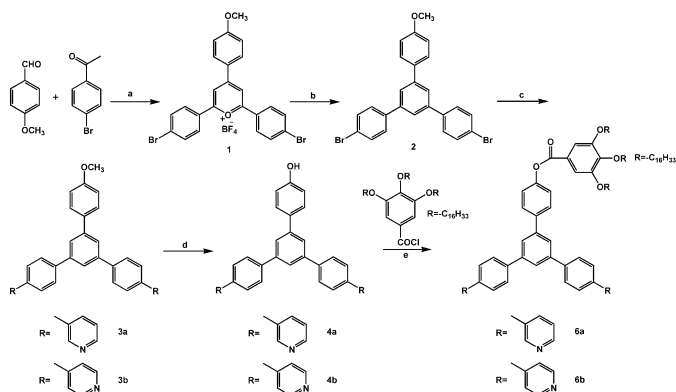
As a significant member of functional soft materials, supramolecular gels have generated enormous interest and become a hot research topic in the past few years.¹ Among them, π -organogelators have gained increasing attention due to their potential applications in many fields, such as organic field effect transistors (OFETs),² photovoltaic devices (PVDs),³ fluorescence imaging and sensing,⁴ etc. π -organogelators can readily self-assemble into stable three dimensional (3D) networks through non-covalent intermolecular interactions such as hydrogen bonding, π - π stacking, dipole-dipole interactions, metal-to-ligand coordination, hydrophobic interactions and so on.^{1e,1g} Because of those complicated and entangled networks, solvent molecules are trapped and immobilized and thus form a jelly-like substance. Since the association of the network of the supramolecular gels system is usually enthalpy driven, most π -organogelators are intrinsically responsive to heat. But with the elaborate artificial modifications on a molecular level, they can be tailor-made to be responsive to other external stimuli, such as light,⁵ pH,⁶ ultrasound,⁷ anion,⁸ metal ion,⁹ etc., which displays more promising applications than conventional polymer networks. Hence, π -organogelators are a clear manifestation of supramolecular chemistry in action and it is still necessary to develop novel π -organogelators with remarkable properties.

The self-assembly of amphiphilic bent-shaped dendrimers containing an extended rigid block and a chiral oligo(ethylene oxide) dendritic segment had been explored extensively in the last decade, especially by M. Lee and coworkers.¹⁰ It has been reported that such a rigid bent-shaped aromatic segments with an internal angle of 120° fit together easily to form non-covalent macrocycles because of the sliding motions between the molecules.^{10e} When pyridine unit was introduced to the both terminals of the bent shaped aromatic segments, metal ion responsive properties were obtained because of the well-known pyridine-metal coordination process, which gave rise to the distinctive nano-structural switch in aqueous solution.^{10d} Such bent-shaped molecules exhibit excellent self-assembly and stimuli-responsive properties. However, to the best of our knowledge, few reports were found with respect to this specific bent-shaped hydrophobic molecules and their application as π -organogelators. This led us to consider building a bent-shaped molecule containing pyridine unit at both ends but with hydrophobic alkyl chains. In this way, the aromatic moiety provided the π - π stacking interaction and the alkyl chains furnish the molecule with hydrophobic interaction, which are favorable for the formation of a gel. While on the other hand, the pyridine segment endow the molecule with stimuli-responsive properties. These could serve as the theoretical foundation of this work.

In this paper, two analogous bent-shaped 3, 5-bis(*m*-(phen-4-yl)pyridine)-1-(4-cresol)yl **3**, 4, 5-tris(hexadecyloxy)benzoate (**6a**) and 3, 5-bis(*p*-(phen-4-yl)pyridine)-1-(4-cresol)yl **3**, 4, 5-tris(hexadecyloxy)benzoate (**6b**) were prepared, which only differ in the position of the N atom at the pyridine ring. It turns out that the

State Key Laboratory of Fine Chemicals, School of Chemical Engineering, Dalian University of Technology, Dalian 610023, PR China. Email: wtong@dlut.edu.cn; ninggl@dlut.edu.cn

*Electronic Supplementary Information (ESI) available: Synthetic procedures, detailed instrumentation, NMR and mass spectra, spectroscopic spectra, computational modelling. See DOI: 10.1039/x0xx00000x



Scheme 1 Synthetic routes of compound **6a** and **6b**. a) $\text{BF}_3 \cdot \text{OEt}_2$; b) CH_3COONa , acetic anhydride; c) 3-pyridinylboronic acid (**3a**) or 4-pyridinylboronic acid (**3b**), $\text{Pd}(\text{PPh}_3)_4$, K_2CO_3 , $\text{THF}/\text{H}_2\text{O}$; d) BBr_3 , dry CH_2Cl_2 ; e) triethylamine, dry CH_2Cl_2 .

slight change of structure has a great influence on their fluorescence as well as gelation capabilities. Theoretical calculations revealed a clear discrepancy of electron distribution between them. More importantly, gelation properties of the two compounds were examined and confirmed by rheological studies. SEM studies were conducted to take a closer look on the morphologies of the xerogels and a hierarchical self-assembly process was observed. Related spectroscopic tests as well as powder X-ray diffraction revealed that **6a** possesses a stronger intermolecular π - π stacking interaction than **6b**. In the end, the application for detecting volatile acid vapours on xerogel films as well as in the gel state was fulfilled through a rare gel to gel transformation. Film **6a** and **6b** showed quite different sensing modes toward acid vapours, which might find potential application as fluorimetric chemosensor for the detection of volatile acid vapours.

Results and Discussion

Synthetic procedures

The structures and synthetic routes of the two investigated compounds **6a** and **6b** are shown in Scheme 1. It is noteworthy that the synthetic method of the bent-shaped core that we applied is quite different from the traditional way starting from the Suzuki coupling reaction of 3, 5-dibromoanisole utilized by M. Lee and coworkers.¹⁰ We started from a classical condensation reaction with anisic aldehyde and *p*-bromoacetophenones under Lewis acid condition ($\text{BF}_3 \cdot \text{OEt}_2$) which gave the substituted 2, 4, 6-triphenyl pyrylium salt. Following a nucleophilic reaction, the substituted 2, 4, 6-triphenylbenzene was generated. Compared with the above-mentioned conventional method, it contains one more benzene ring which is probably more favorable for the intermolecular π - π stacking. Similar synthetic methods had been extensively applied in the synthesis of polycyclic aromatic hydrocarbons (PAHs) and macrocycles described by S. Höger and coworkers,¹¹ but few examples were found with regard to this method employed in constructing supramolecular backbones. The identities of all the new compounds were confirmed by $^1\text{H-NMR}$, $^{13}\text{C-NMR}$ and HRMS, and shown to be in full agreement with the structures presented. In addition, FT-IR spectroscopy were also conducted for **6a** and **6b**. They both exhibited a $\nu(\text{C}=\text{O})$ vibration around 1735 cm^{-1} and $\nu(\text{C}-\text{O})$

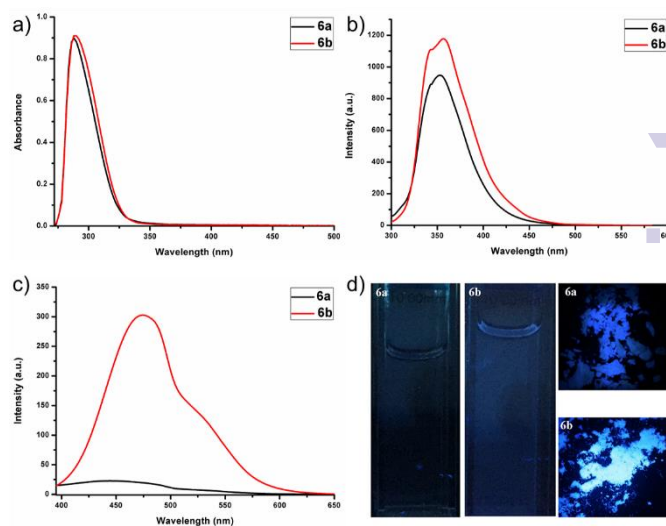


Fig. 1 (a) UV-vis spectra of **6a** and **6b** in THF (0.01 mM); (b) Fluorescence spectra of **6a** and **6b** in THF (0.01 mM, $\lambda_{\text{exc}}=298\text{ nm}$); (c) Fluorescence spectra of **6a** and **6b** in solid state ($\lambda_{\text{exc}}=344\text{ nm}$ and 378 nm , respectively); (d) Fluorescence images of **6a** and **6b** in THF solution (taken under a UV lamp) and in solid state (taken under a fluorescence microscope)

C) vibration around 1190 cm^{-1} , which are the characteristic peaks of an ester group.

Photophysical properties

Spectroscopic properties of **6a** and **6b** in solution and solid state were first investigated, and the data are summarized in Table S1 (ESI[†]). As we can see from Fig. 1a, they both showed a single intense absorption peak around 288 nm, which is assignable to a π - π^* transition. When excited at 298 nm in THF, they both displayed a clear emission peak at around 355 nm while **6b** had a stronger intensity than **6a** (Fig. 1b), with a quantum yield of 13.4% versus 8.5% using 2-aminopyridine in 0.1N H_2SO_4 (quantum yield=60.0%) as the standard sample.¹² When solid fluorescence was investigated, much to our surprise, huge differences were observed. It is clear to see from Fig. 1c that **6b** showed a strong emission at 475 nm ($\lambda_{\text{exc}}=378\text{ nm}$, absolute quantum yield=17.4%) while **6a** exhibited an emission at 444 nm ($\lambda_{\text{exc}}=344\text{ nm}$, absolute quantum yield=0.8%) which is very weak compared with **6b**. The strikingly different emission properties of the two similar compounds suggest that the position of N atom at the pyridine ring plays distinctive roles in each case. It is usually considered that the solid state fluorescence of a compound is strongly dependent on the intermolecular stacking effect (intermolecular distance) and electronic structure.¹³ Therefore it is plausible to deduce that the intermolecular stacking fashion and electronic distribution might be different between **6a** and **6b** in the solid state. Our following experiments also confirmed this point. Also it is noteworthy that for **6b**, the quantum yield of the solid state is even higher than that of liquid, which might indicate an aggregation induced emission (AIE) property of **6b**.¹⁴ The emissive spectra with a varying water volumetric fraction experiment was conducted (Fig. S1, ESI[†]). Interestingly, when the water volumetric fraction in THF/water mixtures increased from 10% to 60%, the fluorescence intensity gradually decreased which suggested a polarity-reduced emission.¹⁴ As the water volumetric fraction enhanced from 60% to 90%, the emission intensity

increased synchronously accompanied by a red shift of emission wavelength and a broader peak, which implied that AIE is responsible for this fluorescence enhancement (Fig. S2, ESI[†]). It is usually considered that the restriction of intramolecular rotations (RIR) blocks the non-radiative pathway and opens up the radiative channel that leads to the AIE phenomenon.¹⁵

Theoretical Calculations

Theoretical studies were conducted to get further insight into the molecular structures and electron distributions of the two compounds. Their geometries and energies were optimized and calculated by density functional theory (DFT) and time-dependent density functional theory (TD-DFT) at the B3LYP/6-31G (d) level. All the hexadecyl chains are replaced by methyl groups for computational simplicity. The optimized ground state geometries of **6a** and **6b** were presented in Fig. S3 (ESI[†]). Generally, very similar conformations were observed. All the benzene rings and pyridine rings in the aromatic moiety are nonplanar with dihedral angles ranging from 140° to 144° (Fig. S4 and Table S2, ESI[†]). The only obvious conformational difference between them is the dihedral angles between the pyridine ring and the proximate benzene ring. **6a** displays a slightly more twisted conformation with dihedral angles of 142.14° and 142.64°, which is smaller than that of **6b** (144.04° and 144.13°).

Closer inspection of the molecular orbitals (MOs), nevertheless, revealed the electronic discrepancy between them. Particularly, a model molecule **6c** that pyridine ring replaced by benzene ring was also studied for a better comparison. As shown in Fig. 2, it is possible to see the for **6a** and **6c**, the density of the HOMO orbital is mainly located in the aromatic parts except for the benzene ring connected with the ester group and the LUMO is more

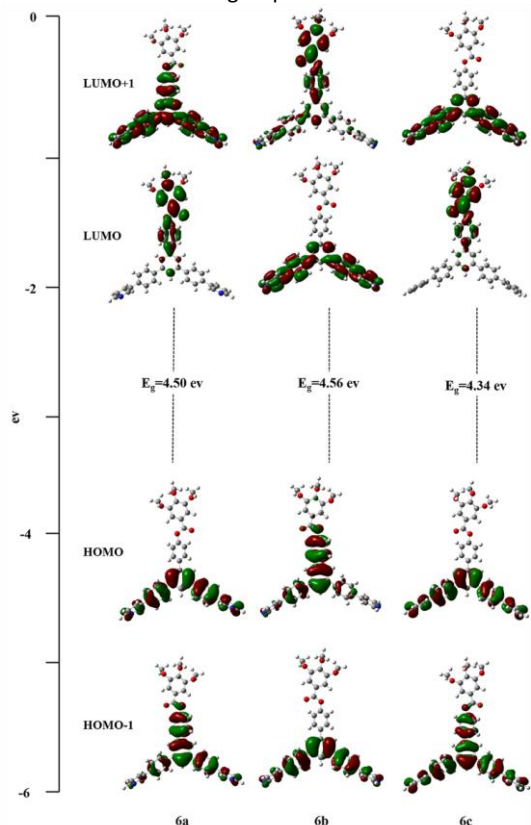


Fig. 2 Selected ground state MOs of **6a**, **6b** and **6c**.

concentrated on the 3, 4, 5- tris(methoxy)benzene and the adjacent benzene ring. However, for **6b**, the situation is totally different. The HOMO is mostly dominated by the central two phenyl rings and the ester group whereas the LUMO resides predominantly on the aromatic parts except for the phenyl ring connected with the ester group. This result suggested that both the aromatic segment and the 3, 4, 5- tris(methoxy)benzene tail (including the ester group) showed significant participation in formation of these electronically important states. However, as for **6a**, the *m*-pyridine ring seems to have little impact on the electron distribution while the *p*-pyridine ring strongly affected the electron distribution of HOMO and LUMO compared with **6c**. The more separated electron distribution of **6a** apparently suggested a more obvious intramolecular charge transfer (ICT) transition than **6b**. In addition, the TD-DFT vertical excitation calculations on the ground state optimized structures helped us to assign the experimental absorption band. For **6a**, the λ_{abs} was associated to the transition from the HOMO-1 to the LUMO+1 with an excitation energy 4.0433 eV (oscillator strength $f=0.0082$), while for **6b**, the λ_{abs} was derived from the HOMO to the LUMO with an excitation energy 4.0143 eV (oscillator strength $f=0.0328$). This also explains the slight absorption red-shift of **6b** compared with **6a**.

Gelation behaviours

Gelation capabilities of **6a** and **6b** were subsequently investigated and compared. Applying a conventional heating-and-cooling method, as we expected, both of them can fulfil the gelation of several common solvents and the results are tabulated in Table S3 (ESI[†]). They can gelate both non-polar solvents (hexane, cyclohexane), polar solvents (dioxane, acetone, DMF) and mixed solvent (DMSO/DCM). However, as we can see from Table S3 (ESI[†]) the gelation behaviours between them are quite different since the solvents that they gelate are not the same. Moreover, the gel of **6a** formed in hexane is translucent while the gel formed in dioxane is opaque (Fig. S5, ESI[†]). The luminescence of the gels are also quite different. The gels of **6b** all showed strong blue fluorescence while for **6a**, the fluorescence of gels are rather weak (Fig. 3), which showed similar rules to their solid states. The gels were quite robust once formed in a capped vial and almost no shrinkage occurred even after standing for a month. Gel-to-solution transition temperature (T_g) showed a synchronous enhancement with concentration in dioxane in a certain range (Fig. S6, ESI[†]). But it is worth mentioning that in non-polar solvents, it usually took a much longer time (over 1 hour) and relatively higher critical gelation concentration (CGC) to form a stable gel while for polar solvents, a stable gel was generated almost immediately upon cooling. This result indicated that polar solvents are more favourable for the effective self-assembly of the molecules. Overall, **6a** showed a better gelation capability than **6b** with 5 gels out of 16 solvents.

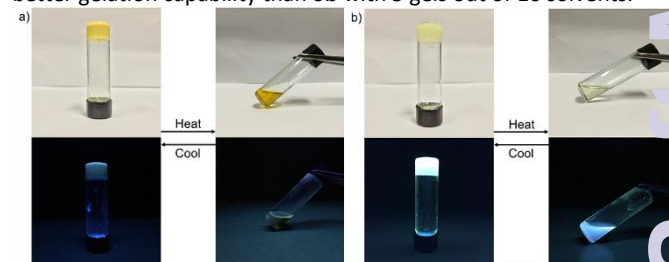


Fig. 3 The gel-to-sol transition of **6a** (a) and **6b** (b) in dioxane (35 mg/mL) and fluorescence images under a UV lamp

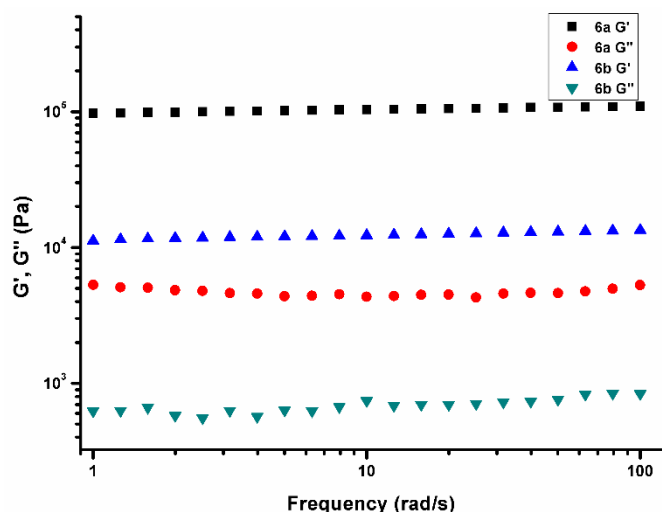


Fig. 4 Frequency sweep for the gels (35 mg/mL) of **6a** and **6b** formed in dioxane (strain=0.05%)

Rheological studies

Viscoelasticity is always one of the most characteristic properties of gels, and the best way to characterize it is rheological studies.¹⁶ A frequency sweep was first carried out to confirm the gel phase. As seen from Fig. 4, for the gel of **6a**, under an applied strain of 0.05%, the storage modulus G' (about 1×10^5 Pa) is much larger than the loss modulus G'' (about 5×10^3 Pa) over the entire range of angular frequency (0.1-100 rad/s), which authenticated the gel state. Furthermore, the G' and G'' almost remained constant with increasing frequency, thereby revealing that the gel showed a good tolerance to external forces. Also, it is noteworthy that the values of G' and G'' of **6a** are much larger than that of **6b** ($G' \sim 1.2 \times 10^4$ Pa, $G'' \sim 7 \times 10^2$ Pa), which suggested that the gel of **6a** formed in dioxane is more robust than **6b** possibly due to stronger intermolecular interaction. G' and G'' were also measured as a function of increasing strain amplitude from 0.01% to 1000% (Fig. S7-S8, ESI[†]). For **6a**, the G' and G'' showed independence of the strain up to a critical strain level of about 0.65%, that is to say, it started to flow at such critical strain value. However, the gel of **6b** began to lose its solid-like behaviour at a critical strain value of 0.16%. The critical strain value of **6a** is evidently larger than that of **6b**, which again proved robustness of the gel of **6a** as compared to the gel of **6b**.

Morphological analysis

Nanostructures self-assembled during the gel formation could be very important because of their potential morphology dependent applications in different areas.¹⁷ To get a more detailed understanding of the self-assembly process that lead to the formation of a gel, morphologies of the dilute solutions (0.1 mM ~1 mM) as well as the xerogels (freeze-dried gels) were examined by scanning electron microscopy (SEM). As we can see from Fig. 5a, in dilute solution (0.1 mM in dioxane), **6a** self-assembled into uneven sizes, discrete vesicles with diameters varying from several hundred nanometres to about 2 μm . The diameters of the observed vesicles were found to much bigger than that of the single molecular size obtained from theoretical calculation (Fig. S9-S10, ESI[†]), which meant that numerous molecules were involved to self-assemble

such a vesicle. As the concentration increased (0.5 mM), vesicles with collapsed interior and larger diameter ranging from 1 μm to about 10 μm were observed (Fig. 5b, 5c). This is probably the consequences of the aggregation of small vesicles. As the concentration reached 1 mM, both fragmented vesicles and tangled layer structure coexisted in a small area (Fig. 5d). This is due to the further aggregation of the collapsed vesicles. Finally, for the xerogel, evident three-dimensional (3D) porous lamellar structure were observed, resulted from the overlap of the layers (Fig. 5e, 5f). **6b** exhibited a similar self-assembly process in dioxane except that thicker, denser layer structure was obtained (Fig. S11, ESI[†]). The gradually structural transformation under different concentrations might provide evidence for a hierarchical build-up of supramolecular assembly,¹⁸ which started from small-sized vesicles at low concentration to larger vesicles at medium concentration to co-existence of vesicles and layered structure at high concentration, and finally give rise to an entangled sample-spanning network that prevents flow of the bulk solvent, as such leading to the gel-type macroscopic behaviour. Even so, differences between the gels formed in different solvents are also evident. For example, for **6a**, SEM studies revealed that the gel obtained from dioxane gave irregular sheet-like layer by layer structures as mentioned above. While in hexane, the gel aggregated into a honeycomb-like structure with numerous pore space. (Fig. S12, ESI[†]). Different from **6a**, for **6b**, the gel formed in dioxane displayed a thick, dense, layer-by-layer structure. However, the gel formed in cyclohexane showed a compact porous morphology (Fig. S13, ESI[†]). The different morphologies formed in different solvents reminded us that the solvent environment can significantly influence the morphologies of

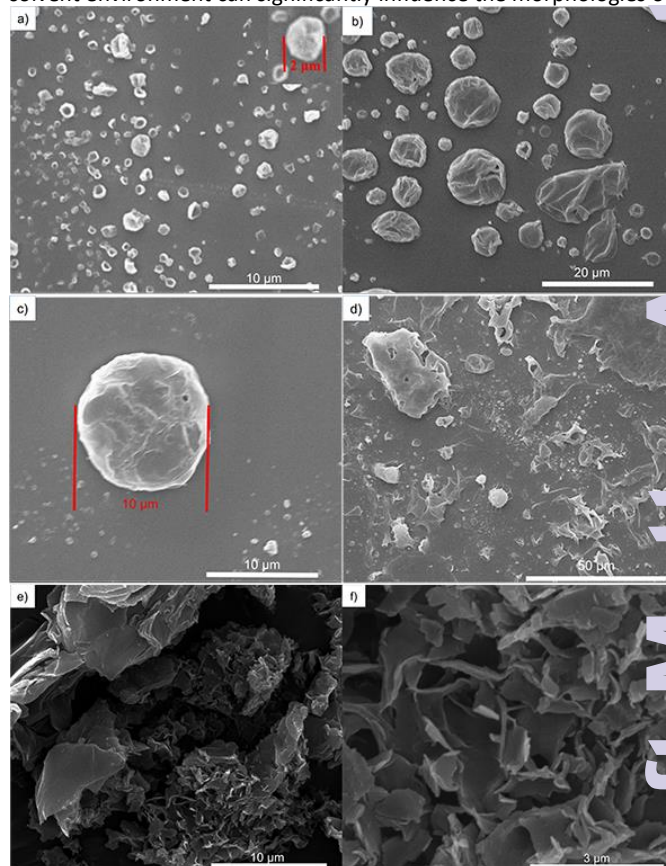


Fig. 5 SEM images of **6a**: (a) 0.1 mM in dioxane; (b, c) 0.5 mM in dioxane with different magnifications; (d) 1 mM in dioxane; (e, f) xerogel obtained in dioxane with different magnifications

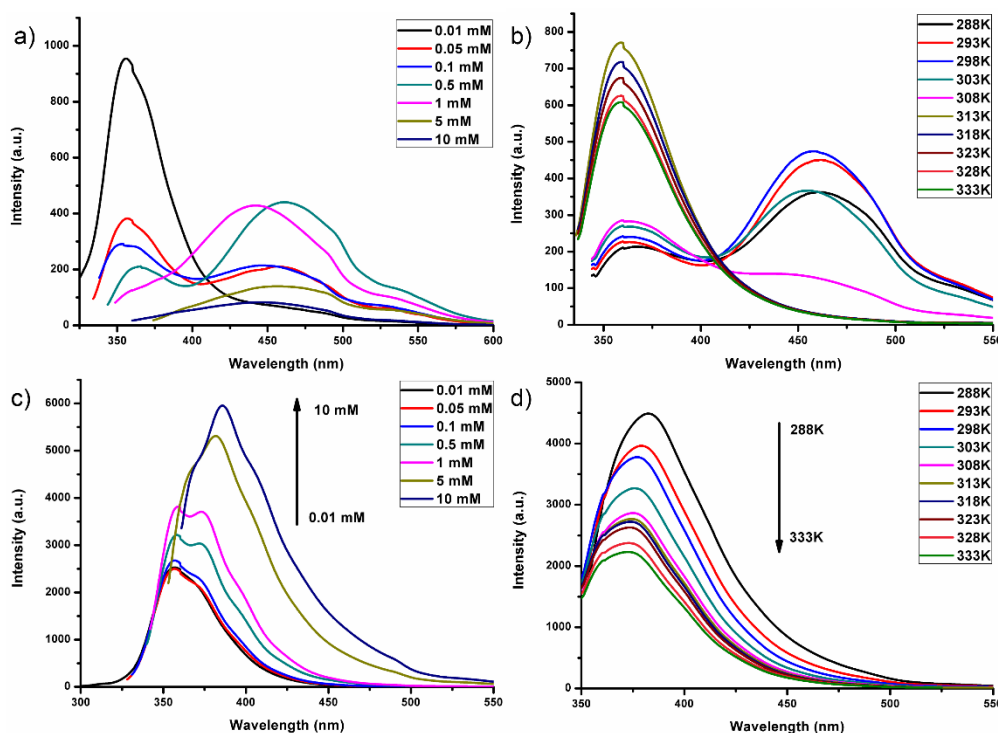


Fig. 6 Concentration and temperature-dependent fluorescence spectra of **6a** (a, b) and **6b** (c, d).

the xerogels which could be attributed to the hydrophobic/hydrophilic nature of the solvents. In all circumstances, it is exactly these 3D network that immobilized the solvent molecules and thus formed a gel.

Spectroscopic tests

Although it is difficult to determine the exact molecular arrangements in the gel state, optical spectra can be a helpful tool to provide relevant information during the self-assembly process. For our system, concentration dependent UV-vis were first studied. It is obvious to see that with increasing concentration, the absorption peak of **6a** and **6b** showed a red-shift of 14 nm and 6 nm, respectively (Fig. S14-S15, ESI[†]). This indicated a stronger intermolecular interactions with increasing concentration. Self-assembly of these two compounds were also indicated by changes in the emission spectra as a function of concentration and temperature (Fig. 6). For example, when monitored in dilute solution (0.01 mM in dioxane), **6a** showed a sharp emission peak at 356 nm, which is the emissive peak of a monomer. Upon increasing concentration, a reduction in the intensity of the high-energy emission band at 356 nm and concomitant increase of a new low-energy emission band at longer wavelength were observed. When the concentration finally reached as high as 10 mM, the peak at 356 nm completely disappeared and only a broad peak centred at 450 nm was observed, which suggested the formation of an aggregated state. The large red-shift in the emission spectra was attributed to the effective aromatic-aromatic interaction, which often led to formation of an excimer between the aromatic segments.¹⁹ Meanwhile, when the temperature was lowered from 333K to 283K, a similar phenomenon was observed, which is consistent with the concentration-dependent emission spectra. For **6b**, with an increasing concentration (0.01 mM to 10 mM in dioxane), the emission peak shifted from 357 nm to 386 nm, accompanied by a

much stronger intensity, which might suggested the formation of J aggregates.²⁰ Temperature-dependent emission spectra showed a comparable transformation. It is worth mentioning that the red-shift of **6a** (94 nm) is apparently much larger than that of **6b** (29 nm), which indicated a much stronger π - π interaction between the aromatic moieties. This also explains the robustness difference of the gels as mentioned in the rheology studies. The temperature and concentration induced changes in the optical spectra of the two compounds revealed a clear association with the self-assembly process, which suggested that the rigid bent-shaped aromatic core played an important role in this process.

Variable concentration ¹H-NMR

To detect the delicate π - π stacking interaction during the self-assembly, variable concentration ¹H-NMR has always been a powerful method. Though both **6a** and **6b** failed to gelate in chloroform at room temperature as shown in Table S3 (ESI[†]), concentration-dependent ¹H-NMR in pure deuterated chloroform (CDCl₃) at room temperature was observed. For **6a**, with an increasing concentration from 2mM to 32mM, the aromatic protons depicted an obvious upfield shift as much as 0.073 ppm (Fig. 7) which indicated that the electrons in the molecule experienced larger shielding effect, therefore suggested π - π stacking during the self-assembly process. In addition, it was observed that different aromatic protons showed different extents of upfield shifts, for which H_c and H_d on the pyridine ring, showed the largest extent of upfield shifts compared with the protons on the benzene rings, which might indicated a much stronger π - π stacking interaction between the pyridine rings. Similar phenomenon was found for **6b** (Fig. S16, ESI[†]). Therefore, the formation of the gels was driven by π - π stacking of the aromatic segment and hydrophobic interaction of long alkyl chains.

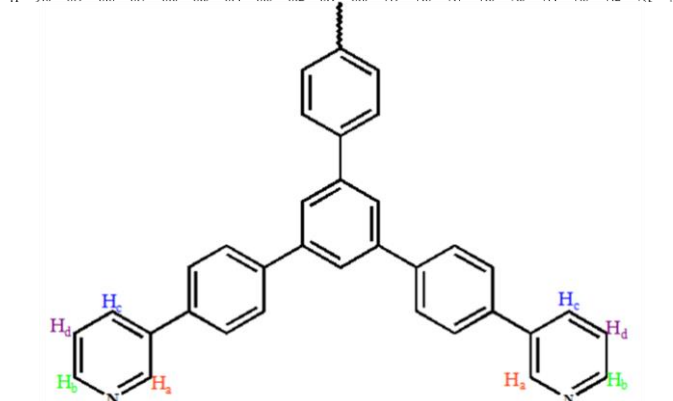
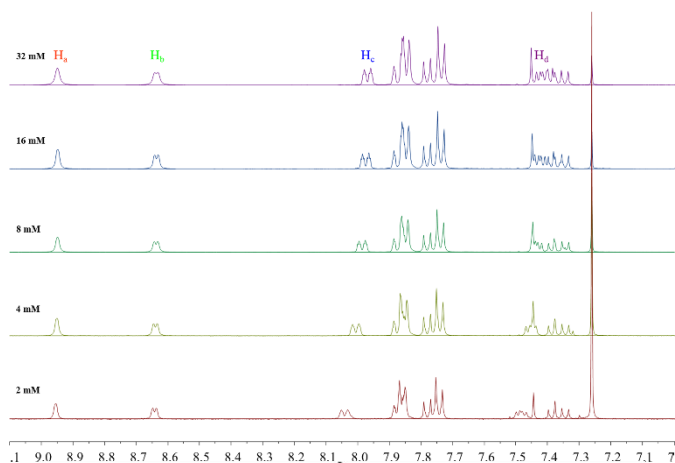


Fig. 7 Concentration-dependent ^1H NMR spectra of **6a** ranging from 2 mM to 32 mM in CDCl_3 at room temperature (only aromatic region) (up) and the labelled protons on the pyridine ring of **6a** (down).

Powder X-ray diffraction

The aggregation behaviour of the xerogels of **6a** and **6b** were also analysed by powder X-ray diffraction (PXRD). In the wide angle region, though both of them showed a diffraction peak related to π - π stacking interaction, difference was observed. The xerogel of **6a** showed a diffraction peak around 23.5° indicating an intermolecular separation of $d=0.38$ nm (Fig. 8). However for the xerogel of **6b**, the diffraction peak centred at around 21.1° corresponding to an intermolecular separation of $d=0.42$ nm (Fig. S17, ESI †). The peak of **6a** was slightly sharper, and the d value was smaller compared with **6b**, which suggested closer packing mode that led to stronger π - π stacking interactions. This result is consistent with the spectroscopic tests and rheological studies above.

Detecting volatile acid vapours

Considering that sp^2 -hybridized N atom is a good proton acceptor and the 3D network formed in gels permits the rapid diffusion of analytes which is beneficial for a fast response, the response of **6a** and **6b** upon exposure to acid vapours were tested qualitatively. Due to the strong acidity and volatility of trifluoroacetic acid (TFA), it was first utilized as our analyte. The protonation of **6a** and **6b** by excess TFA was first confirmed by ^1H -NMR. As shown in Fig. S18 and

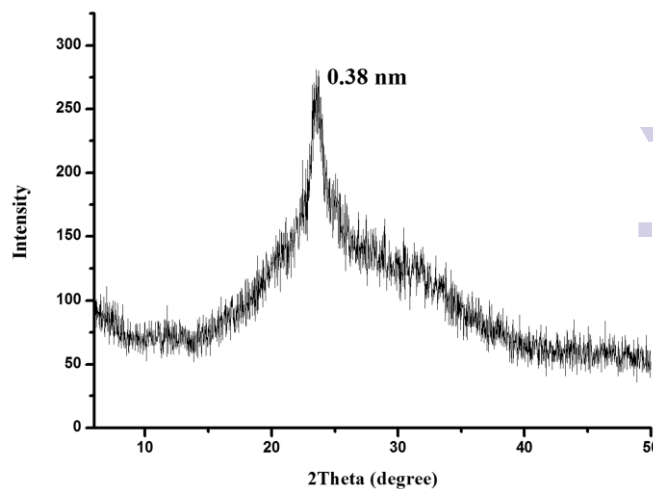


Fig. 8 PXRD spectrum of the xerogel of **6a** obtained from dioxane

S19 (ESI †), all the protons on the pyridine ring clearly went through a large down field shift as much as 0.7 ppm, which indicated the protonation of the pyridine ring. Then the response of **6a** and **6b** to TFA was studied in the solution first. The UV-vis spectra change of **6a** (0.01 mM in THF) upon addition of excess TFA showed that the absorption wavelength stayed the same only with an absorbance shifting from 0.9 to 1.31 (Fig. S20, ESI †), which suggested that the protonation of **6a** (**P6a**) did not affect the electron energy level of the molecule. The fluorescence emission spectra revealed a clear red-shift changing from 370 nm to 416 nm meanwhile the intensity almost remained unchanged (Fig. S21, ESI †). This result indicated that monomer **P6a** is as emissive as **6a** but with a longer emission wavelength. **6b** showed analogous phenomenon upon addition of excess TFA, with the same absorption wavelength but an emission wavelength shifting from 373 nm to 421 nm (Fig. S22-S23, ESI †). However, since the fluorescence intensity of **P6a** and **P6b** in dilute solution is rather weak, the change in the emission spectra with addition of TFA can hardly be observed by naked eye under a UV lamp, which limited the application for detecting TFA in solution.

To improve the feasibility of detecting TFA with **6a** and **6b**, two xerogel films were prepared. Interestingly, the films showed quite different response modes compared with their solutions (Fig. 9). For **6a**, before exposing to TFA vapour, the fluorescence of the film was very weak which showed an emission peak at 435 nm. Upon exposure to TFA for 3 seconds, the film showed a strong blue fluorescence centred at 464 nm accompanied by a 5-fold intensity enhancement, which can easily be seen under a UV lamp. While for **6b**, the film showed a strong blue fluorescence centred at 463 nm before exposure to TFA, which is similar to the solid fluorescence. After that, the emission peak shifted to 489 nm and an evident yellow-green fluorescence was observed. The results implied that both films of **6a** and **6b** could fulfil the detection of TFA vapour based on a fluorescence change not only in colour but also in intensity. In addition, other common acid vapours including HCl , HNO_3 , H_2SO_4 and CH_3COOH were also tested. As we can see from Fig. S24 and S25 (ESI †), all of them showed similar phenomenon only with a slight difference in emission wavelength and intensity. Except that, the response to H_2SO_4 required a much longer time possibly due to the slow evaporation rate of H_2SO_4 vapour.

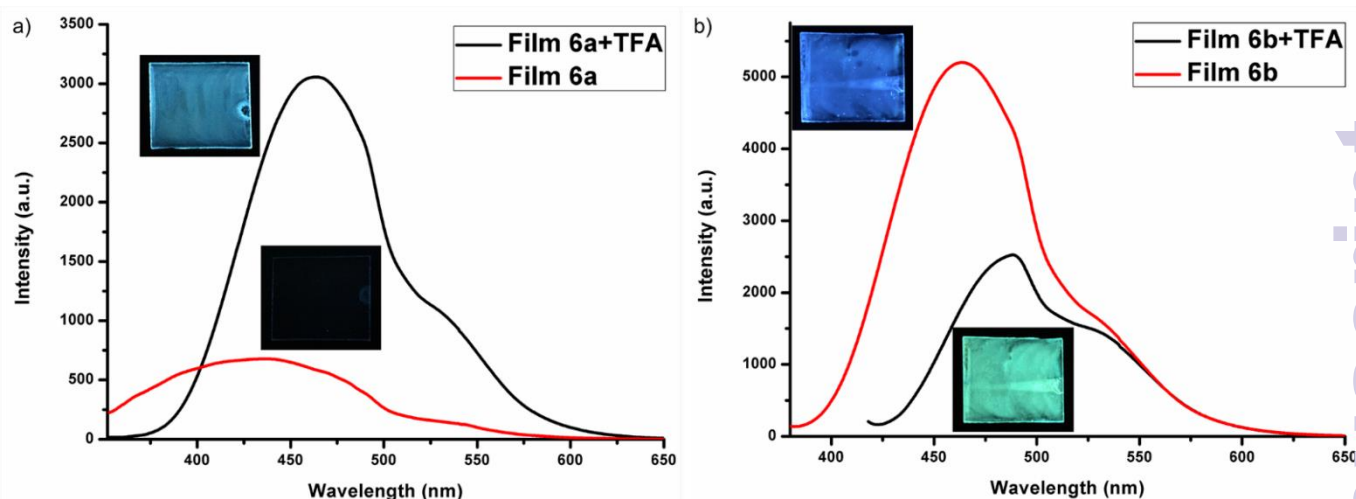


Fig. 9 Fluorescence spectra of film **6a** (a) and **6b** (b) before and after exposing to TFA vapour

The reversibility of the films was also examined to check the endurance of the films as chemosensors. Both the fluorescence intensity and emission wavelength of the films can be recovered to the original level by exposing to triethylamine (TEA) vapour for 3 seconds. Such a protonation-deprotonation process on the film can be repeated for multiple times without obvious deamplification (Fig. S26-S31, ESI[†]), indicating excellent reversibility. This enhances the potential of this system as fluorimetric sensing of acid vapours.

Inspired by the interesting responsiveness of the two films to acid vapours, we further investigated the responsiveness of the wet gels

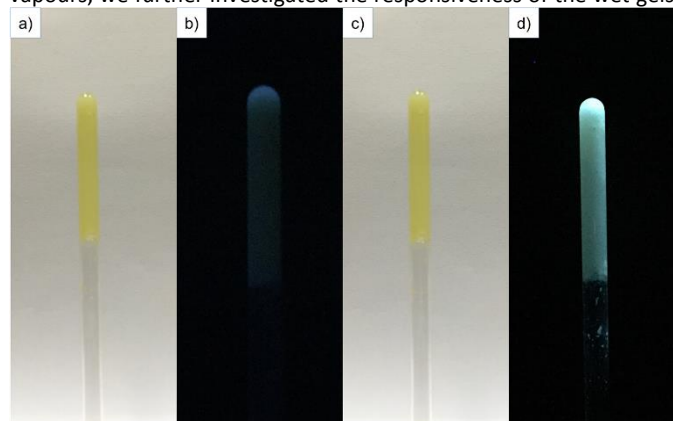


Fig. 10 The daylight images of the gel of **6a** before (a) and after (c) exposure to TFA; The fluorescence images of the gel of **6a** before (b) and after (d) exposure to TFA

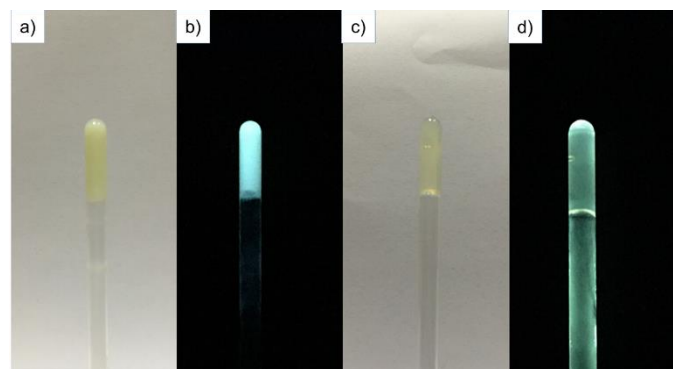


Fig. 11 The daylight images of the gel of **6b** before (a) and after (c) exposure to TFA; The fluorescence images of the gel of **6b** before (b) and after (d) exposure to TFA

to TFA vapour. Much to our surprise, instead of the usual collapse of the gel network along with a strong blue fluorescence similar to the film (Fig. 10). SEM study of the xerogel of **6a** after protonation revealed a denser and thicker laminar structure (Fig. S32, ESI[†]). The wet gel of **6b** in dioxane also showed a gel to gel transformation accompanied with a fluorescence change (Fig. 11) and morphology alteration (Fig. S33, ESI[†]). More interestingly, the gel became translucent after addition of TFA. It is important to stress that, to the best of our knowledge, such a vapour stimuli-responsive gel to gel transformation is rather rare only with a few reports found.²¹ In most cases, the introduce of an external stimulus into a gel would weaken the non-covalent interactions and destroy the entangled network.

Conclusions

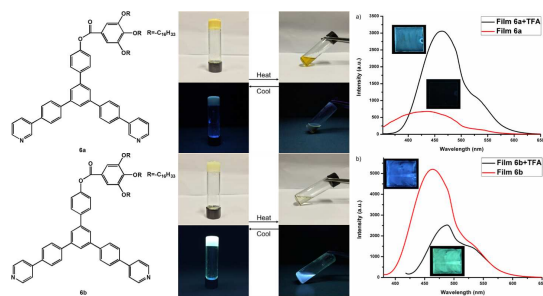
In summary, we have synthesized two hydrophobic bent-shaped bis-pyridine compounds **6a** and **6b**. The photophysical properties of them were measured and discussed. **6a** with an *m*-pyridine unit showed very weak fluorescence in solid state while **6b** with a *p*-pyridine unit exhibited very strong fluorescence. Theoretical studies were conducted to help understanding the molecular structures and electron distribution of these two compounds, which revealed an obvious difference between them. Gelation capabilities of **6a** and **6b** were studied and confirmed by rheology studies. However, the wet gel of **6b** showed strong luminescence while the wet gel of **6a** was almost non-emissive. The morphology studies revealed a hierarchical self-assembly process and a solvent-dependent morphology relationship. Rheological studies, spectroscopic tests and powder X-ray diffraction showed that **6a** displayed a close packing mode which led to stronger gel robustness. In the end, two xerogel films prepared from these two gels were utilized to detect acid vapour qualitatively which showed different response modes through a rare gel to gel transformation. Excellent reversibility of the films were observed, which might find potential applications as fluorimetric chemosensor for the detection of volatile acid vapours.

Acknowledgements

The authors are grateful for financial support from the National Natural Science Foundation of China (NO.21206016) and the Fundamental Research Funds for the Central Universities (DUT14LK08).

Notes and references

- a) P. Terech, R. G. Weiss, *Chem. Rev.* **1997**, *97*, 3133-3159; b) M. George, R. W. Weiss, *Accounts. Chem. Res.* **2006**, *39*, 489-497; c) H. Maeda, *Chem. Eur. J.* **2008**, *14*, 11274-11282; d) X. Yan, F. Wang, B. Zheng, F. Huang, *Chem. Soc. Rev.* **2012**, *41*, 6042-6065; e) S. S. Babu, S. Prasanthkumar, A. Ajayaghosh, *Angew. Chem. Int. Ed.* **2012**, *51*, 1766-1776; f) A. Y. Y. Tam, V. W. W. Yam, *Chem. Soc. Rev.* **2013**, *42*, 1540-1567; g) S. S. Babu, V. K. Praveen, A. Ajayaghosh, *Chem. Rev.* **2014**, *114*, 1973-2129.
- a) J. P. Hong, M. C. Um, S. R. Nam, J. I. Hong, S. Lee, *Chem. Commun.* **2009**, 310-312; b) R. J. Kumar, J. M. MacDonald, T. B. Singh, L. J. Waddington, A. B. Holmes, *J. Am. Chem. Soc.* **2011**, *133*, 8564-8573; c) W. W. Tsai, I. D. Tevis, A. S. Tayi, H. Cui, S. I. Stupp, *J. Phys. Chem. B.* **2010**, *114*, 14778-14786.
- a) M. Koppe, C. J. Brabec, S. Heimpl, A. Schausberger, W. Duffy, M. Heeney, I. McCulloch, *Macromolecules*, **2009**, *42*, 4661-4666; b) P. Xue, R. Lu, L. Zhao, D. Xu, X. Zhang, K. Li, Z. Song, X. Yang, M. Takafuji, H. Ihara, *Langmuir*, **2010**, *26*, 6669-6675; c) B. G. Kim, E. J. Jeong, H. J. Park, D. Bilby, L. J. Guo, J. Kim, *ACS Appl. Mater. Interfaces.* **2011**, *3*, 674-680.
- a) J. W. Chung, S. J. Yoon, S. J. Lim, B. K. An, S. Y. Park, *Angew. Chem. Int. Ed.* **2009**, *48*, 7030-7034; b) K. K. Kartha, S. S. Babu, S. Srinivasan, A. Ajayaghosh, *J. Am. Chem. Soc.* **2012**, *134*, 4834-4841; c) S. Srinivasan, P. A. Babu, S. Mahesh, A. Ajayaghosh, *J. Am. Chem. Soc.* **2009**, *131*, 15122-15123; d) N. Dey, S. K. Samanta, S. Bhattacharya, *ACS Appl. Mater. Interfaces.* **2013**, *5*, 8394-8400; e) P. Xue, J. Sun, B. Yao, P. Gong, Z. Zhang, C. Qian, Y. Zhang, R. Lu, *Chem. Eur. J.* **2015**, *21*, 4712-4720.
- a) K. Murata, M. Aoki, T. Suzuki, T. Harada, H. Kawabata, T. Komori, F. Ohseto, K. Ueda, S. Shinkai, *J. Am. Chem. Soc.* **1994**, *116*, 6664-6676; b) N. Koumura, M. Kudo, N. Tamaoki, *Langmuir*, **2004**, *20*, 9897-9900; c) S. C. Wei, M. Pan, K. Li, S. Wang, J. Zhang, C. Y. Su, *Adv. Mater.* **2014**, *26*, 2072-2077; d) Q. Chen, Y. Feng, D. Zhang, G. Zhang, Q. Fan, S. Sun, D. Zhu, *Adv. Funct. Mater.* **2010**, *20*, 36-42; e) J. J. D. de Jong, L. N. Lucas, R. M. Kellogg, J. H. van Esch, B. L. Feringa, *Science*. **2004**, *304*, 278-281; f) S. Wang, W. Shen, Y. Feng, H. Tian, *Chem. Commun.* **2006**, 1497-1499; g) R. Rajaganesh, A. Gopal, T. M. Das, A. Ajayaghosh, *Org. Lett.* **2012**, *14*, 748-751.
- a) J. L. Pozzo, G. M. Clavier, J. P. Desvergne, *J. Mater. Chem.* **1998**, *8*, 2575-2577; b) F. R. Llansola, B. Escuder, J. F. Miravet, D. H. Merino, I. W. Hamley, C. J. Cardin, W. Hayes, *Chem. Commun.* **2010**, 46, 7960-7962; c) J. W. Chung, B. K. An, S. Y. Park, *Chem. Mater.* **2008**, *20*, 6750-6755.
- a) K. Isozaki, H. Takaya, T. Naota, *Angew. Chem. Int. Ed.* **2007**, *46*, 2855-2857; b) T. Naota, H. Koori, *J. Am. Chem. Soc.* **2005**, *127*, 9324-9325; c) D. Bardelang, F. Camerel, J. C. Margeson, D. M. Leek, M. Schmutz, M. B. Zaman, K. Yu, D. V. Soldatov, R. Ziessel, C. I. Ratcliffe, J. A. Ripmeester, *J. Am. Chem. Soc.* **2008**, *130*, 3313-3315; d) J. M. Malicka, A. Sandeep, F. Monti, E. Bandini, M. Gazzano, C. Ranjith, V. K. Praveen, A. Ajayaghosh, N. Armaroli, *Chem. Eur. J.* **2013**, *19*, 12991-13001.
- a) C. Wang, D. Zhang, D. Zhu, *Langmuir*. **2007**, *23*, 1478-1482; b) P. Rajamalli, E. Prasad, *Org. Lett.* **2011**, *13*, 3714-3717; c) C. E. Stanley, N. Clarke, K. M. Anderson, J. A. Elder, J. T. Lenthall, J. W. Steed, *Chem. Commun.* **2006**, 3199-3201; d) Z. X. Liu, Y. Feng, Z. Y. Zhao, Z. C. Yan, Y. M. He, X. J. Luo, C. Y. Liu, Q. H. Fan, *Chem. Eur. J.* **2014**, *20*, 533-541; e) Q. Lin, T. T. Lu, X. Zhu, B. Sun, Q. P. Yang, T. B. Wei, Y. M. Zhang, *Chem. Commun.* **2015**, *51*, 1635-1638; f) Y. Liu, N. Zheng, H. Li, B. Yin, *Soft Matter*. **2013**, *9*, 5261-5269.
- a) Q. Jin, L. Zhang, X. Zhu, P. Duan, M. Liu, *Chem. Eur. J.* **2012**, *18*, 4916-4922; b) E. M. Schön, E. M. López, R. P. Herrera, C. Alemán, D. D. Díaz, *Chem. Eur. J.* **2014**, *20*, 10720-10731; c) N. V. Lakshmi, D. Mandal, S. Ghosh, E. Prasad, *Chem. Eur. J.* **2014**, *20*, 9002-9011.
- a) H. J. Kim, W. C. Zin, M. Lee, *J. Am. Chem. Soc.* **2004**, *126*, 7009-7014; b) H. J. Kim, J. H. Lee, M. Lee, *Angew. Chem. Int. Ed.* **2005**, *44*, 5810-5814; c) H. J. Kim, J. K. Kim, M. Lee, *Chem. Commun.* **2010**, 46, 1458-1460; d) S. Shin, S. Lim, Y. Kim, T. Kim, T. L. Choi, M. Lee, *J. Am. Chem. Soc.* **2013**, *135*, 2156-2159; e) Z. Huang, S. K. Kang, M. Banno, T. Yamaguchi, D. Lee, C. Seok, E. Yashima, M. Lee, *Science*. **2012**, *337*, 1521-1526.
- a) S. Höger, S. Rosselli, A. D. Ramminger, V. Enkelmann, *Org. Lett.* **2002**, *4*, 4269-4272; b) X. H. Cheng, S. Höger, D. Fenske, *Org. Lett.* **2003**, *5*, 2587-2589; c) C. Mahler, U. Müller, W. M. Müller, V. Enkelmann, C. Moon, G. Brunklauer, H. Zimmermann, S. Höger, *Chem. Commun.* **2008**, 4816-4818; d) G. Ohlendorf, C. W. Mahler, S. S. Jester, G. Schnakenburg, S. Grimme, S. Höger, *Angew. Chem. Int. Ed.* **2013**, *52*, 12086-12090.
- R. Rusakowicz, A. C. Testa, *J. Phys. Chem.* **1968**, *72*, 2680-2681.
- a) H. Langhals, T. Potrawa, H. Nöth, G. Linti, *Angew. Chem. Int. Ed. Engl.* **1989**, *28*, 478-480; b) N. S. S. Kumar, S. Varghese, C. H. Suresh, N. P. Rath, S. Das, *J. Phys. Chem. C.* **2009**, *113*, 11927-11935; c) K. Yokota, M. Hagimori, N. Mizuyama, Y. Nishiruma, H. Fujito, Y. Shigemitsu, Y. Tominaga, *Beilstein. J. Org. Chem.* **2012**, *8*, 266-274.
- S. Sasaki, K. Igawa, G. Konishi, *J. Mater. Chem. C.* **2015**, *3*, 5940-5950.
- a) Y. Hong, J. W. Y. Lam, B. Z. Tang, *Chem. Soc. Rev.* **2011**, *40*, 5361-5388; b) J. Mei, Y. Hong, J. W. Y. Lam, A. Qin, Y. Tang, B. Z. Tang, *Adv. Mater.* **2014**, *26*, 5429-5479.
- a) M. O. M. Piepenbrock, G. O. Lloyd, N. Clarke, J. W. Steed, *Chem. Rev.* **2010**, *110*, 1960-2004; b) G. Yu, X. Yan, C. Han, F. Huang, *Chem. Soc. Rev.* **2013**, *42*, 6697-6722.
- L. Zhang, X. Wang, T. Wang, M. Liu, *Small*. **2015**, *11*, 1025-1038.
- N. S. S. Kumar, S. Varghese, G. Narayan, S. Das, *Angew. Chem. Int. Ed.* **2006**, *45*, 6317-6321.
- T. Förster, *Angew. Chem. internat. Edit.* **1969**, *8*, 333-343.
- a) H. Yao, K. Domoto, T. Isohashi, K. Kimura, *Langmuir*. **2005**, *21*, 1067-1073; b) F. Würthner, T. E. Kaiser, C. R. Saha-Möller, *Angew. Chem. Int. Ed.* **2011**, *50*, 3376-3410.
- a) H. Lee, S. H. Jung, W. S. Han, J. H. Moon, S. Kang, J. Y. Lee, J. H. Jung, S. Shinkai, *Chem. Eur. J.* **2011**, *17*, 2823-2827; b) S. Bhattacharya, S. Sengupta, S. Bala, A. Goswami, S. Ganguly, R. Mondal, *Cryst. Growth Des.* **2014**, *14*, 2365-2374.



A slight difference in the position of N atom on the pyridine ring greatly affect fluorescence, gelation and sensing properties!